Enhanced absorption in two-dimensional materials via Fano-resonant photonic crystals

Wenyi Wang,[1] Andrey Klots,[2] Yuanmu Yang,[3] Wei Li,[4] Ivan I. Kravchenko,[5] Dayrl P. Briggs,[5] Kirill I. Bolotin,[2] and Jason Valentine[4,a)]
[1]*Department of Electrical Engineering and Computer Science, Vanderbilt University, Nashville, Tennessee 37212, USA*
[2]*Department of Physics and Astronomy, Vanderbilt University, Nashville, Tennessee 37240, USA*
[3]*Interdisciplinary Materials Science Program, Vanderbilt University, Nashville, Tennessee 37212, USA*
[4]*Department of Mechanical Engineering, Vanderbilt University, Nashville, Tennessee 37212, USA*
[5]*Center for Nanophase Materials Sciences, Oak Ridge National Laboratory, Oak Ridge, Tennessee 37831, USA*

(Received 1 March 2015; accepted 20 April 2015; published online 5 May 2015)

The use of two-dimensional (2D) materials in optoelectronics has attracted much attention due to their fascinating optical and electrical properties. However, the low optical absorption of 2D materials arising from their atomic thickness limits the maximum attainable external quantum efficiency. For example, in the visible and near-infrared regimes monolayer MoS_2 and graphene absorb only ~10% and 2.3% of incoming light, respectively. Here, we experimentally demonstrate the use of Fano-resonant photonic crystals to significantly boost absorption in atomically thin materials. Using graphene as a test bed, we demonstrate that absorption in the monolayer thick material can be enhanced to 77% within the telecommunications band, the highest value reported to date. We also show that the absorption in the Fano-resonant structure is non-local, with light propagating up to 16 μm within the structure. This property is particularly beneficial in harvesting light from large areas in field-effect-transistor based graphene photodetectors in which separation of photo-generated carriers only occurs ~0.2 μm adjacent to the graphene/electrode interface. © *2015 AIP Publishing LLC*. [http://dx.doi.org/10.1063/1.4919760]

Two-dimensional (2D) materials with exceptional optical and electrical properties are promising for use in the next generation of optoelectronic devices. For instance, graphene has been proven to have ultrahigh charge mobility[1] and broadband absorption,[2] which has led to ultrafast[3–8] and broadband photodetectors.[9,10] Its unique cone-like electronic band structure also allows one to actively tune the absorption through electrostatic gating, allowing realization of high-speed modulators.[11] Monolayer semiconducting transition metal dichalcogenides (TMDCs), such as MoS_2, are more preferable materials for photodetectors due to their direct band gap and internal amplification, and they have been employed as ultrasensitive photodetectors with photoresponsivities up to 880 A/W.[12] However, the efficiency of 2D material-based optoelectronic devices is typically limited by their poor optical absorption, a feature which is a direct consequence of their atomic thickness. For instance, a single pass through MoS_2, with a thickness 6–7 Å,[13] results in a peak absorption of ~10% at 660 nm.[14] Graphene, whose thickness is 3 Å, absorbs 2.3% of the incident light[2] and only responds to light with the electric field component polarized parallel to the atomic plane. Several methods have been reported to enhance the absorption in 2D materials, and particularly in graphene, including patterning graphene into periodic arrays[15] and integrating it with plasmonic structures[16,17] or microcavities.[18,19] Among these methods, the highest graphene absorption that has been realized experimentally in the near-infrared or visible regime was accomplished using microcavities where 60% absorption was achieved.[19]

In this letter, we demonstrate that absorption in 2D materials can be significantly enhanced by incorporating them into a Fano-resonant photonic crystal (FRPC, Figure 1(a)), which consists of a photonic crystal slab exhibiting Fano resonances, or guided resonances[20–23] and a silver back reflector to completely block the transmission. This type of structure has recently been examined theoretically with a perfect mirror as the back reflector,[24] and 85% total absorption was experimentally measured though the portion of absorption occurring in graphene, opposed to the portion in the back reflector, was not measured.[25] Here, we implement the FRPC with both graphene and MoS_2. For the graphene-integrated FRPC (Gr-FRPC), in addition to showing 96% total absorption, we experimentally demonstrate that graphene absorbs 77% of the incident light within the telecommunications band. This is the highest graphene absorption demonstrated experimentally in the telecommunications band, to the best of our knowledge. Moreover, we experimentally show that the absorption in the FRPC is a non-local effect, namely, light can propagate in the structure to as far as 16 μm from the illumination point before being absorbed. For graphene-based field effect transistor (GFET) photodetectors, non-local absorption opens up a new route to increase the external quantum efficiency which suffers from the fact that electrons and holes are only separated within a ~0.2 μm region adjacent to the electrodes[26] in the absence of an external bias or photothermoelectric effects.

a)Email: jason.g.valentine@vanderbilt.edu

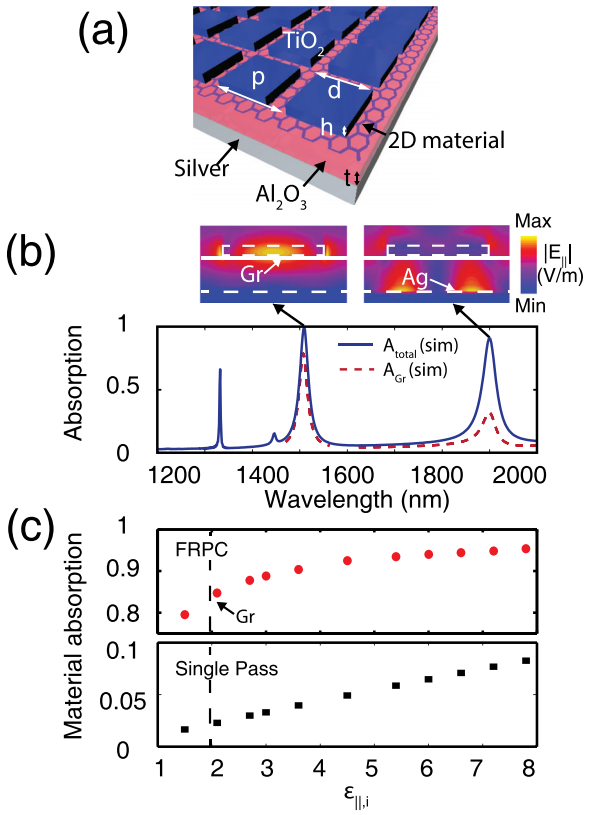

FIG. 1. (a) Schematic of the Fano-resonant photonic crystal. (b) Total absorption (solid line) and the absorption in graphene (dashed line) at normal incidence and the in-plane E-field ($|E_{||}|$) distribution at the vertical cross section of the structure at the first resonance mode near 1900 nm (upper right) and the second mode at 1507 nm (upper left). (c) Absorption within different 2D materials when integrated with a FRPC structure resonant at 540 nm (upper) and the single pass absorption (lower) as a function of the imaginary part of the in-plane component of the permittivity ($\varepsilon_{||,i}$) at the same wavelength.

Figure 1(a) shows the schematic of the FRPC structure. In order to increase absorption, it is essential to achieve modal overlap of the in-plane electric field and the 2D material. This goal is achieved by using the Fano resonance[20] in photonic crystal slabs. In these Fano resonances, a guided resonance mode excited in the photonic crystal interferes with the free space mode, creating a Fano line shape in the transmission and reflection spectra.[21–23] Furthermore, we employ a silver back reflector to block transmission, allowing absorption to approach unity. The back reflector is spaced from the photonic crystal (PC) slab (composed of TiO_2 cubes) by an Al_2O_3 spacer layer, and the 2D material is sandwiched between the Al_2O_3 and the PC slab. A weak Fabry-Perot cavity is then formed between the silver mirror and the PC slab, providing a broadband reflectance spectrum. Interference occurs between the PC modes and the Fabry-Perot resonance, resulting in sharp Fano resonance peaks, which reduces to a Lorentzian line shape when the direct transmission is zero, as is the case here.[21,22] The thickness of the Al_2O_3 is chosen such that spectral overlap of the two modes is achieved.

The normal-incident total absorption spectrum of a Gr-FRPC structure ($p = 1370$ nm, $d = 950$ nm, $h = 120$ nm, $t = 275$ nm) is shown in Figure 1(b). While two absorption modes in Figure 1(b) exhibit total absorption approaching unity, at the first resonance mode located at 1900 nm, graphene absorbs only 31.8% of the light while silver absorbs 59.2%. These values were obtained by multiplying the material loss with the integration of the E-field within graphene and the metal separately. The enhancement of absorption in silver rather than in graphene is a result of the E-field being confined near the silver back reflector (Figure 1(b), right field profile). In contrast, at the second band located at 1507 nm (Figure 1(b), left field profile), the in-plane E-field is highly confined at the interface between Al_2O_3 and the PC slab, resulting in 79% of the incident light being absorbed within graphene. The graphene absorption spectrum around the two resonant modes are presented in Figure 1(b) with dashed lines, and remainder of this letter will be focused on examining the second resonant mode which exhibits high absorption enhancement in graphene.

Other than graphene, the FRPC performs equally well in the visible regime and for a wide range of 2D materials with varied absorptivity. In Figure 1(c) (upper panel), the second resonance mode has been scaled to a wavelength of 540 nm and 2D materials with in-plane imaginary permittivities ($\varepsilon_{||,i}$) ranging from 1.5 to 7.8 are embedded into the FRPC structure. Graphene absorbs 84.7% at the resonance peak while absorption rises up to 95% for materials with larger loss. The single pass absorption of these 2D materials is provided in the lower panel of Figure 1(c) for reference.

To experimentally demonstrate the absorption enhancement in 2D materials, Gr-FRPC and MoS_2-FRPC were fabricated. For proof of principle experiments, graphene was chosen due to its relatively poor absorption compared to TMDCs, thus representing the worst-case scenario, while MoS_2 is selected as a representative of TMDCs that absorb in the visible regime. Monolayer CVD graphene (confirmed by Raman spectroscopy), or monolayer exfoliated MoS_2, were transferred onto a Al_2O_3/silver stack, and a TiO_2 photonic crystal with an area of 100 μm × 100 μm was defined on top. Images of a fabricated FRPC structure designed for graphene and a MoS_2-FRPC device are shown in Figures 2(a) and 2(b), respectively. In the MoS_2-FRPC, the flake is smaller than the array and sits at the center.

The response of the FRPC structure is sensitive to the angle of incidence (see supplementary material Figure S1[27]) and to account for this dependence, the optical absorption of the Gr-FRPC was measured with light confined to within ±2.5° normal to the substrate (see Figure S2[27] for the optical set-up). A tunable diode laser with full width half maximum (FWHM) less than 200 kHz (New Focus 6326) was used as the laser source and reflection from the center of the array (R) was measured, yielding the absorption, $A = 1 - R$. A peak absorption of 96% was obtained at 1507 nm and matches well with the simulation (Figure 2(c)). The absorption of bare graphene sitting on the same Al_2O_3/silver stack, but without the PC, was measured to be 8.5%, also matching the simulation.

For the MoS_2-FRPC, the resonance is designed to be at 538 nm ($p = 387$ nm, $d = 172.2$ nm, $h = 46$ nm, $t = 203.5$ nm). In this case, 16 nm of PMMA was spun on top of the device to perfectly match the resonance wavelength with the laser. The solid red and blue curves in Figure 2(d) are the simulated total FRPC absorption and absorption within MoS_2 as a function of

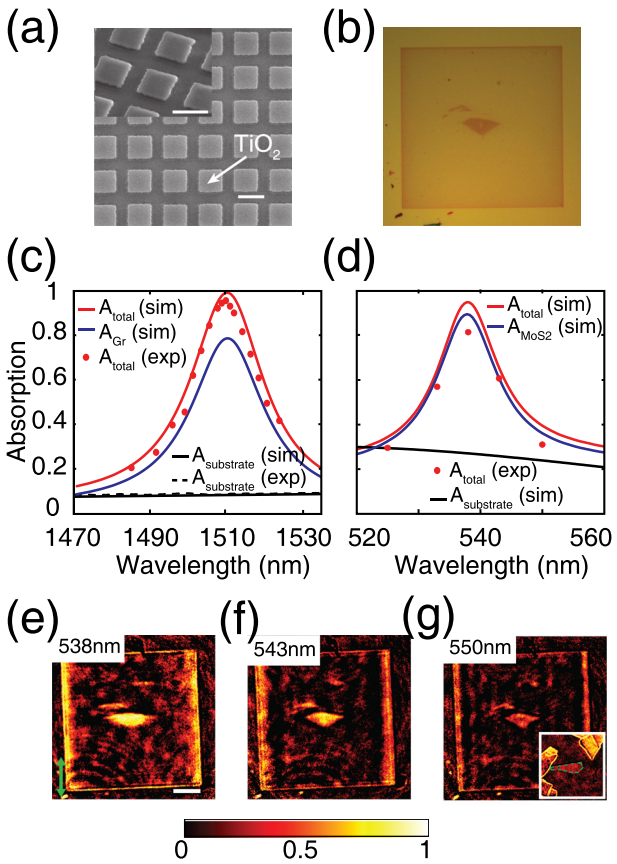

FIG. 2. (a) SEM of the fabricated FRPC designed for graphene, scale bar = 1 μm. (b) Microscope image of the MoS_2-FRPC with a MoS_2 flake at the center. (c) Experimentally measured absorption of the Gr-FRPC and bare graphene on the substrate (Al_2O_3/silver stack). (d) Experimentally measured absorption of the MoS_2-FRPC. (e)–(g) Absorption maps of the MoS_2-FRPC array shown in (b) at various wavelengths. The inset of (g) shows the absorption map of bare MoS_2 on the substrate (the monolayer MoS_2 flake is marked by a green dash line). The green arrow in (e) indicates the incident light polarization and the scale bar is equal to 20 μm.

wavelength, showing values of 95% and 90% at the resonance peaks, respectively. This is higher than in the case of graphene as MoS_2 is more absorptive in this wavelength range. The fact that the small piece of MoS_2 is embedded in the FRPC array allows us to directly visualize the absorption enhancement in MoS_2 by illuminating the entire array with a collimated laser at various wavelengths, both on and off resonance. A map of absorption is obtained by comparing the reflectance intensity obtained from the MoS_2-FRPC and from a mirror, as is shown in Figure 2(e) (on resonance), and 2(f) and 2(g) (off resonance). The absorption values from the center of FRPC array where MoS_2 is present were extracted and are plotted with red dots in Figure 2(d). The illumination laser has a FWHM of 3–4 nm, and the measured absorption is the average value within this bandwidth, lowering the measured value compared to the simulation. For comparison, the inset of Figure 2(g) shows a map of bare MoS_2 on top of Al_2O_3/silver illuminated at 538 nm with a measured absorption of 24.6%, closely matching the simulation value, which is ~25% in this wavelength range.

While the total absorption enhancement in the Gr-FRPC and MoS_2-FRPC clearly indicate strong light-matter interaction, these measurements do not allow us to experimentally validate the percentage of absorption in the 2D materials. To extract this information, we measured the photocurrent from a Gr-FRPC device and compared the result with the photocurrent from bare graphene sitting on top of the same Al_2O_3/silver stack. The schematic of the photodetector device is shown in Figure 3(a). A source drain bias of $V_{sd} = -4.1$ V was applied over a 180 μm long channel with a channel width of 210 μm to negate the variations in the Fermi level due to doping non-uniformities that resulted from the fabrication process. Note that the DC current was measured to be $I_{DC} \sim 1.1$ mA, resulting in an electrical power density of $\sim 12\ W/cm^2$, which is small enough to avoid significant Joule heating of the film.[28] A gate voltage of $V_G = 60$ V was used to ensure that the Pauli blocking is not active.[29] The device was illuminated in the middle of the Gr-FRPC array, and a reference measurement was taken on bare graphene (points A and B in Figure 3(a)). The incident laser beam, with a spot size greater than 15 μm and the E-field polarized parallel to the electrodes, was located 50 μm away from the nearest electrode. The illumination power was kept low so that the power absorbed by graphene is less than 35 μW. With this setup, the measured photocurrent is a result from photovoltaic and bolometric effects,[30] both of which increase by the same amount due to the enhanced absorption. The current from the thermoelectrical effect[31] is negligible due to the fact that this effect is based on the difference in the Seebeck coefficient between two different regions, which is negligible under the applied source-drain voltage. The photocurrent as a function of incident power is provided in Figure S4.[27]

The experimentally measured photocurrent from the device, $I_{FRPC}(\lambda)$, and from bare graphene, $I_{Gr}(\lambda)$, are shown in Fig. 3(b), with the peak current occurring at $\lambda_0 = 1507$ nm, matching well with the shape of the simulated graphene absorption. Comparison of $I_{FRPC}(\lambda)$ to the mean value of $I_{Gr}(\lambda)$ yields an experimental photocurrent enhancement factor F_I of 14.33 at $\lambda = \lambda_0$ with $F_I(\lambda)$ defined as $I_{FRPC}(\lambda)/\overline{I_{Gr}(\lambda)}$ (red dots in Figure 3(c)). As a reference, the theoretical absorption within graphene for the case of a bare film sitting on the same Al_2O_3/silver stack, defined as $Abs_{bare}(\lambda)$, is 5.23% at 1510 nm with an average value from 1480 nm to 1530 nm of 5.4% (solid line in the inset of Figure 3(b). These values yield a theoretical graphene absorption enhancement factor $F_{Abs}(\lambda_0)$ of 14.63, where $F_{abs}(\lambda) = Abs_{FRPC}(\lambda)/\overline{Abs_{bare}(\lambda)}$ (black line in Figure 3(c)) and $Abs_{FRPC}(\lambda)$ is the graphene absorption when it is embedded in the FRPC. The measured photocurrent enhancement factor $F_I(\lambda_0)$ is close to the simulated absorption enhancement $F_{Abs}(\lambda_0)$ and indicates that 77% of the light is being absorbed within the graphene layer at the resonance peak, which is obtained using the relationship

$$Abs_{FRPC,exp}(\lambda_0) = \frac{F_I(\lambda_0)}{F_{Abs}(\lambda_0)} Abs_{FRPC,sim}(\lambda_0). \quad (1)$$

The same enhancement is also observed when the E-field is perpendicular to the electrodes (see Figure S5[27]).

Another key feature of our structure is that absorption is non-localized due to propagation within the photonic crystal. Opposed to conventional photonic crystal cavities where light is confined within a small volume, photons in the FRPC are confined vertically to a thin region near the 2D material but are free to propagate in the lateral direction. Figure 4(a)

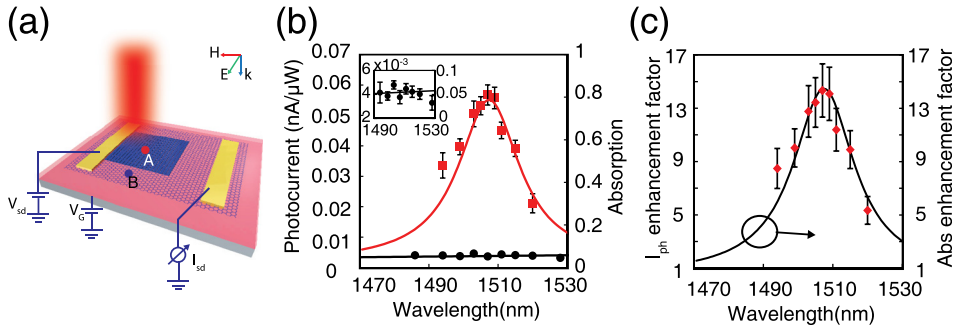

FIG. 3. (a) Schematic of the Gr-FRPC photodetector device. (b) Photocurrent from the center of the Gr-FRPC array (point A) (red dots) and on bare graphene, corresponding to point B (black dots). The red and black solids lines correspond to the simulated graphene absorption in the FRPC and on an Al_2O_3/silver substrate, respectively. Inset: zoom in of the graphene photocurrent and simulated graphene absorption for the case of bare graphene. (c) Photocurrent enhancement factor $F_I(\lambda)$ (dots) and the graphene absorption enhancement factor $F_{Abs}(\lambda)$(line).

shows the intensity of the in-plane electric field ($|E_{||}|^2$) when a Gaussian beam with a $1/e^2$ half-width of $w_{gaus}/2 = 4.5\,\mu$m and E_y polarization is incident on a FRPC that has not been integrated with a 2D material. The excitation of the TE mode with E_y and H_z components results in the field spreading out in the x direction, as can be observed in Figure 4(a). Fitting the envelope of the field intensity along the white dashed line gives a Lorentzian line shape with a half width in the x direction of 28.4 μm, indicating that light propagates $\sim$24 μm away from the spot of incidence. The intensity profile along the grey dashed line matches a Gaussian line shape whose half width is 5.6 μm.

To demonstrate non-local absorption experimentally, we scanned a laser beam with a $1/e^2$ half width of 4.5 μm over a FRPC that was partially covered by graphene. The sample was broken down into 3 regions, as is shown in simulated absorption profile A_{sim} (inset of Figure 4(b)), where region I consists of the FRPC, without graphene, region II consists of the FRPC with graphene, and region III is void of the FRPC.

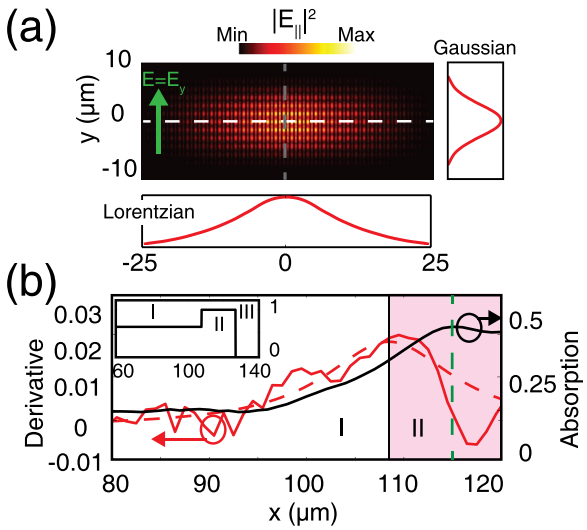

FIG. 4. (a) Intensity plot of the in-plane electric field ($|E_{||}|^2$) distribution when a Gaussian beam with a $1/e^2$ half width of 4.5 μm is incident on the FRPC without graphene. The two curves on the bottom and right are envelopes of $|E_{||}|^2$ taken along the white and grey dashed lines within the FRPC, respectively. (b) Measured absorption (black line) and the derivative of absorption (red line) near the region I/II border. Red dashed line shows the fit to the derivative. The inset depicts the simulated normal incidence absorption of the entire array A_{sim}.

Absorption in region I is soley due to ohmic loss in the metal back plane while absorption in region II is dominated by graphene. Due to the finite beam size and propogation within the PC, the measured absorption is blurred as the beam travels from regions I into II (black line Figure 4(b)). The blurring process is a convolution between the field profile and the A_{sim}, and it can be shown that the derivative of the measured absorption, as a function of position, is proportional to the field distribution in the FRPC array (details are discussed in Sec. 7 of the the supplementary material). The derivative of the measured absorption is shown in Figure 4(b) (red line), and the data to the left of the green dashed line (x = 115 μm) are fitted with a Lorentzian curve (red dashed line). To the right of the green dashed line, the response of the FRPC is dominated by the unpatterned area (region III) and absorption begins to dip. From the fit to the derivative of absorption, we obtain an intensity distribution whose $1/e^2$ half width within the FRPC is 20.7 μm, indicating a propagation distance of $\sim$16 μm from the incident spot. This value is slightly smaller than the calculated value of 24 μm and the error most likely arises from defects within the FRPC due to fabrication imperfections and contamination from the graphene transfer process. It should also be noted that the simulated propagation distance in region II is only 8.9 μm due to the existence of graphene which introduces a larger non-radiative decay rate. This indicates that in our photocurrent enhancement measurements (Figure 3) light is not making it to the electrodes, but rather being absorbed within the FRPC and thus the current enhancement is due to absorption enhancement rather than more effective charge collection.

In summary, we have experimentally demonstrated that optical absorption in 2D materials as thin as a monolayer of graphene can be increased to 77% by integrating the material within Fano-resonant photonic crystals. Furthermore, the same structure is able to enhance absorption in other 2D materials in the visible regime with absorption in the 2D material reaching values of up to 90% in the case of MoS_2. We also demonstrated that the FRPC structure can be utilized to collect photons incident 16 μm away from the 2D material flake thus increasing the effective detection area, which is typically limited by the flake size. This concept could lead to long channel graphene-based FET photodetectors with greatly enhanced external quantum efficiency while still maintaining an ultrafast photoresponse.

This work was funded by a Vanderbilt University Discovery Grant and the Office of Naval Research (ONR) under programs N00014-12-1-0571, N00014-14-1-0475, and N00014-13-10299. A portion of this research was conducted at the Center for Nanophase Materials Sciences, which is a DOE Office of Science User Facility. A portion of this work was also performed in the Vanderbilt Institute of Nanoscale Science and Engineering (VINSE), we thank the staff for their support.

[1]K. I. Bolotin, K. J. Sikes, Z. Jiang, M. Klima, G. Fudenberg, J. Hone, P. Kim, and H. L. Stormer, Solid State Commun. **146**, 351 (2008).
[2]R. R. Nair, P. Blake, A. N. Grigorenko, K. S. Novoselov, T. J. Booth, T. Stauber, N. M. R. Peres, and A. K. Geim, Science **320**, 1308 (2008).
[3]A. Urich, K. Unterrainer, and T. Mueller, Nano Lett. **11**, 2804 (2011).
[4]F. Xia, T. Mueller, Y.-M. Lin, A. Valdes-Garcia, and P. Avouris, Nat. Nanotechnol. **4**, 839 (2009).
[5]D. Sun, G. Aivazian, A. M. Jones, J. S. Ross, W. Yao, D. Cobden, and X. Xu, Nat. Nanotechnol. **7**, 114 (2012).
[6]T. Mueller, F. Xia, and P. Avouris, Nat. Photonics **4**, 297 (2010).
[7]A. Pospischil, M. Humer, M. M. Furchi, D. Bachmann, R. Guider, T. Fromherz, and T. Mueller, Nat. Photonics **7**, 892 (2013).
[8]X. Gan, R.-J. Shiue, Y. Gao, I. Meric, T. F. Heinz, K. Shepard, J. Hone, S. Assefa, and D. Englund, Nat. Photonics **7**, 883 (2013).
[9]B. Y. Zhang, T. Liu, B. Meng, X. Li, G. Liang, X. Hu, and Q. J. Wang, Nat. Commun. **4**, 1811 (2013).
[10]C.-H. Liu, Y.-C. Chang, T. B. Norris, and Z. Zhong, Nat. Nanotechnol. **9**, 273 (2014).
[11]M. Liu, X. Yin, E. Ulin-Avila, B. Geng, T. Zentgraf, L. Ju, F. Wang, and X. Zhang, Nature **474**, 64 (2011).
[12]O. Lopez-Sanchez, D. Lembke, M. Kayci, A. Radenovic, and A. Kis, Nat. Nanotechnol. **8**, 497 (2013).
[13]D. Jariwala, V. K. Sangwan, L. J. Lauhon, T. J. Marks, and M. C. Hersam, ACS Nano **8**, 1102 (2014).
[14]J.-T. Liu, T.-B. Wang, X.-J. Li, and N.-H. Liu, J. Appl. Phys. **115**, 193511 (2014).
[15]S. Thongrattanasiri, F. H. L. Koppens, and F. J. G. de Abajo, Phys. Rev. Lett. **108**, 047401 (2012).
[16]T. J. Echtermeyer, L. Britnell, P. K. Jasnos, A. Lombardo, R. V. Gorbachev, A. N. Grigorenko, A. K. Geim, A. C. Ferrari, and K. S. Novoselov, Nat. Commun. **2**, 458 (2011).
[17]Y. Liu, R. Cheng, L. Liao, H. Zhou, J. Bai, G. Liu, L. Liu, Y. Huang, and X. Duan, Nat. Commun. **2**, 579 (2011).
[18]M. Engel, M. Steiner, A. Lombardo, A. C. Ferrari, H. V. Löhneysen, P. Avouris, and R. Krupke, Nat. Commun. **3**, 906 (2012).
[19]M. Furchi, A. Urich, A. Pospischil, G. Lilley, K. Unterrainer, H. Detz, P. Klang, A. M. Andrews, W. Schrenk, G. Strasser, and T. Mueller, Nano Lett. **12**, 2773 (2012).
[20]U. Fano, Phys. Rev. **124**, 1866 (1961).
[21]S. Fan, W. Suh, and J. D. Joannopoulos, J. Opt. Soc. Am. A **20**, 569 (2003).
[22]S. Fan and J. Joannopoulos, Phys. Rev. B **65**, 235112 (2002).
[23]J. Lee, B. Zhen, S.-L. Chua, W. Qiu, J. D. Joannopoulos, M. Soljačić, and O. Shapira, Phys. Rev. Lett. **109**, 067401 (2012).
[24]J. R. Piper and S. Fan, ACS Photonics **1**, 347 (2014).
[25]Y. Liu, A. Chadha, D. Zhao, J. R. Piper, Y. Jia, Y. Shuai, L. Menon, H. Yang, Z. Ma, S. Fan, F. Xia, and W. Zhou, Appl. Phys. Lett. **105**, 181105 (2014).
[26]T. Mueller, F. Xia, M. Freitag, J. Tsang, and P. Avouris, Phys. Rev. B **79**, 245430 (2009).
[27]See supplementary material at http://dx.doi.org/10.1063/1.4919760 for (1) simulation and material modelling. (2) Photonic band structure of the Gr-FRPC. (3) Optical setup for the absorption measurement. (4) Fabrication of the Gr-FRPC photodetectors. (5) Measured photocurrent from Gr-FRPC as a function of incident laser power. (6) Enhancement of photocurrent for the E-field perpendicular to the electrodes. (7) Extraction of the electric field distribution from the scanned absorption. (8) Absorption within the FRPC vs. incident angle.
[28]M. Freitag, M. Steiner, Y. Martin, V. Perebeinos, Z. Chen, J. C. Tsang, and P. Avouris, Nano Lett. **9**, 1883 (2009).
[29]R. N. Zitter, Appl. Phys. Lett. **14**, 73 (1969).
[30]M. Freitag, T. Low, F. Xia, and P. Avouris, Nat. Photonics **7**, 53 (2013).
[31]N. M. Gabor, J. C. W. Song, Q. Ma, N. L. Nair, T. Taychatanapat, K. Watanabe, T. Taniguchi, L. S. Levitov, and P. Jarillo-Herrero, Science **334**, 648 (2011).